Multiobjective co-optimization of cooperative adaptive cruise control and energy management strategy for PHEVs

He, Yinglong; Zhou, Quan; Makridis, Michail; Mattas, Konstantinos; Li, Ji; Williams, Huw; Xu, Hongming

DOI:
10.1109/TTE.2020.2974588

Multi-objective Co-optimization of Cooperative Adaptive Cruise Control and Energy Management Strategy for PHEVs

Yinglong He, Quan Zhou, Michail Makridis, Konstantinos Mattas, Ji Li, Huw Williams, and Hongming Xu

***Abstract*—Electrification, automation, and connectivity in the automotive and transport industries are gathering momentum, but there are escalating concerns over their need for co-optimization to improve energy efficiency, traffic safety, and ride comfort. Previous approaches to these multi-objective co-optimization problems often overlook trade-offs and scale differences between the objectives, resulting in misleading optimizations. To overcome these limitations, this study proposes a Pareto-based framework that demonstrably optimizes the system parameters of the cooperative adaptive cruise control (CACC) and the energy management strategy (EMS) for PHEVs. The high-level Pareto knowledge assists in finding a best-compromise solution. The results of this work suggest that the energy and the comfort targets are harmonious, but both conflict with the safety target. Validation using real-world driving data shows that the Pareto optimum for CACC and EMS systems, relative to the baseline, can reduce energy consumption (by 7.57 %) and tracking error (by 68.94 %), while simultaneously satisfying ride comfort needs. In contrast to the weighted-sum method, the proposed Pareto method can optimally balance and scale the multiple objective functions. In addition, sensitivity analysis proves that the vehicle reaction time impacts significantly on tracking safety, but its effect on energy saving is trivial.**

***Index Terms*—Cooperative adaptive cruise control, energy management strategy, multi-objective co-optimization, tracking safety, energy consumption.**

I. Introduction

ENERGY, environmental and safety challenges are exacerbated by rising transport demand [1]. To tackle these problems, vehicle electrification, automation and connectivity are gathering momentum worldwide [2]–[4], but there are escalating concerns over their synergistic impacts on the control design of vehicles that fuse mechatronics with new informatics, such as plug-in hybrid electric vehicles (PHEVs) with automated driving systems.

PHEVs are widely promoted as an efficient and clean solution that combines an internal combustion engine (ICE) with an electric motor and a large rechargeable battery. This hybrid powertrain enables all-electric driving for extended periods of time and overcomes the concern of range anxiety [5], [6]. Intensive efforts on PHEVs have developed energy management strategies (EMS) for coordinating the power split in a fuel-efficient way [7]. However, the performance of EMS is often compromised by the complexity and uncertainty of driving conditions. It is therefore desirable to synergize internal powertrain coordination and external driving behaviour [8]. Meanwhile, the longitudinal driving task gradually shifts from the human driver to in-vehicle automated systems. For example, the radar-aided adaptive cruise control (ACC) and the communication-enabled cooperative adaptive cruise control (CACC) can regulate the vehicle speed to maintain a user-specified time headway or reach the user-desired speed [9]–[11]. These automated driving systems are designed to improve energy efficiency, road safety, and traffic throughput by optimizing velocity trajectories (i.e., eco-driving), which can be integrated with the EMS to further boost fuel economy [12]. Consequently, the co-optimization of CACC/ACC and EMS is gaining traction among automakers and policymakers [13].

Vehicles operate in the three longitudinal driving modes of free-flow, car-following and platooning. Accordingly, studies on CACC/ACC and EMS co-optimization can be divided into the following three groups [14]:

1) Studies for free-flow scenarios [15]–[17] usually deal with road constraints such as speed limits, traffic lights, and road intersections. For example, a powertrain and speed integrated control was proposed to achieve 5.0 - 16.9 % fuel economy benefits, by utilizing the road topography and the dynamic speed limit [18]. Predictive energy optimization for connected and automated PHEVs was reported to deliver a fuel saving of 10.1 % when considering the benefits of traffic light phasing [19].
2) Studies for car-following scenarios [20]–[22] mainly address constraints of the movement of the preceding vehicle, to improve fuel economy, tracking safety, etc. For instance, a predictive car-following power management system for PHEVs was demonstrated to simultaneously coordinate battery state-of-charge (SoC) planning, inter-vehicle spacing, and power split in a cost-optimal manner [23]. Adopting similar techniques, a deep fusion method with ACC and EMS claimed to reduce fuel consumption by 5 % [24].

Manuscript received October 17, 2019; revised December 23, 2019; accepted February 3, 2020. (*Corresponding author: Hongming Xu.*)

Y. He, Q. Zhou, J. Li, H. Williams and H. Xu are with the Department of Mechanical Engineering, the University of Birmingham, Birmingham, B15 2TT, UK. (email: yxh701@bham.ac.uk, q.zhou@bham.ac.uk, h.williams.5@bham.ac.uk, h.m.xu@bham.ac.uk)

M. Makridis and K. Mattas are with the Directorate for Energy, Transport and Climate Change, European Commission - Joint Research Centre (JRC), 2749 - 21027 Ispra (VA), Italy. (email: michail.makridis@ec.europa.eu, konstantinos.mattas@ext.ec.europa.eu)

Digital Object Identifier XX.XXXX/TTE.XXXX.XXXXXXX

3) Studies for platooning scenarios [25], [26] are primarily concerned with interactions between multiple vehicles. In a study on integrated optimization of internal powertrain energy management and external driving coordination for multiple hybrid electric vehicles (HEVs), the optimal results indicated a fuel saving of 17.9 % compared with their baseline counterparts [27]. A two-layer hierarchical control system was constructed for a set of connected HEVs on a hilly terrain [28]. The top layer was tasked with cooperative driving and battery SoC planning; the bottom layer determined the power split and the gear shifting strategy.

From the perspective of objective functions, prior studies on CACC/ACC and EMS co-optimization problems are classified into the following two types:

1) Some studies investigate single-objective co-optimization [29], [30], which generally minimizes fuel consumption by optimizing speed trajectory and power split. However, this can only satisfy the fuel economy needs, neglecting comprehensive vehicle performance improvements.
2) Other studies highlight multi-objective co-optimization [22]–[24], addressing various needs including energy efficiency, tracking safety, ride comfort, traffic throughput, etc., especially in car-following and platooning scenarios. Previous studies converted the original CACC/ACC and EMS co-optimization with multiple objectives into a single-objective optimization problem by weighted-sum methods. For example, in a nonlinear model predictive control (NMPC) system, the safety and the energy targets are integrated into a cost function using a two-dimensional (2D) weight vector [21].

The weighted-sum methods cannot, however, determine the weights and the normalization factors that can optimally balance and scale the multiple objective functions for a problem with little or no information [31], which can cause misleading optimization results. For example, in a study on multi-objective ACC and EMS co-optimization [32], the weighted-sum method led to an over-optimized fuel economy (a fuel saving of 7.07 %), which in turn compromised other attributes such as tracking safety (a tracking error increase of 10.5 %).

To overcome these limitations, we propose a Pareto-based framework dealing with the multi-objective CACC and EMS co-optimization for PHEVs. The high-level knowledge (e.g., trade-offs and scale differences between objectives) of the Pareto frontier (PF) assists in finding a best-compromise solution. The results of this study suggest that the energy and the comfort targets are harmonious but both conflict with the safety target. These objective values are measured on different scales. In the validation using real-world driving data, the Pareto optimum for CACC and EMS systems, compared with the baseline scheme, can reduce energy consumption (by 7.57 %) and tracking error (by 68.94 %), while simultaneously satisfying ride comfort needs. In contrast to the weighted-sum method, the Pareto method can optimally balance and scale the multiple objective functions and thus accurately capture the decision maker's preferences. In addition, sensitivity analysis proves that the vehicle reaction time impacts significantly on tracking safety, but its effect on energy saving is trivial.

The rest of this paper is structured as follows. Section II describes the integrated CACC and EMS control framework as well as the augmented system dynamics for car-following and power-split. Section III presents the multi-objective problem and optimization methods. In Section IV, optimization results from the Pareto and the weighted-sum methods are compared. Section V concludes the paper by summarizing the main findings.

II. Augmented System Dynamics and Integrated Control Framework

Fig. 1 illustrates the integrated CACC and EMS control framework as well as the augmented system dynamics for car-following and power-split. Their mathematical models are elaborated below.

A. Longitudinal Driving Dynamics

The longitudinal motion dynamics of the following vehicle are described by the equations,

$$\begin{cases} v_f = \dot{x_f}, \\ a_f = \dot{v_f}, \\ m_0 a_f = \dfrac{1}{r} T_d - \dfrac{1}{2}\rho C_d A_f v_f^2 - f m_0 g \cos\theta \\ \qquad\qquad - m_0 g \sin\theta, \end{cases} \tag{1}$$

where x_f, v_f and a_f denote the longitudinal position (m), velocity (m/s) and acceleration (m/s^2), respectively; r is the wheel radius (m); T_d represents the driving torque (N·m) on the wheel axle; m_0 is the vehicle operating mass (kg); ρ is the air density (kg/m^3); C_d stands for the air drag coefficient; A_f is the vehicle effective frontal area (m^2); θ is the road slope (rad); g is the gravitational constant (9.8 m/s^2); and f is the rolling resistance coefficient.

B. Cooperative Adaptive Cruise Control

According to CACC systems reported in previous studies [33], [34], the acceleration demand, a_f, can be computed based on the inter-vehicle spacing and the relative speed, a_f^n, or on the difference between the actual speed and the maximum safe speed, a_f^m. Consequently, the following vehicle adopts the more restrictive choice as follows:

$$\begin{cases} a_f(t) = \min\Big(a_f^n(t), a_f^m(t)\Big), \\ a_f^n(t) = a_l(t-\tau) + k_v\Big(v_l(t-\tau) - v_f(t-\tau)\Big) \\ \qquad\qquad + k_s\Big(s(t-\tau) - s_{des}\Big), \\ a_f^m(t) = \Big(v_f^{max} - v_f(t)\Big)/t_s, \end{cases} \tag{2}$$

where a_l and v_l are the leading vehicle's acceleration (m/s^2) and speed (m/s), respectively. τ denotes the reaction time (s)

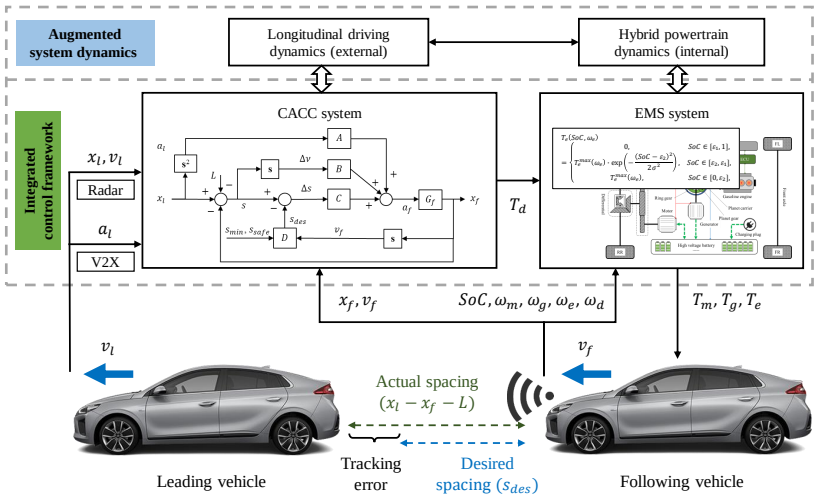

Fig. 1. The augmented system dynamics and the integrated control framework.

including communication, sensing and actuation delays. Here t_s represents the control sample time (0.1 s); s is the bumper-to-bumper spacing (m); s_{des} is the desired inter-vehicle spacing (m); v_f^{max} is the maximum safe speed (m/s); and k_v and k_s are gain factors to minimize the speed difference and the tracking error, respectively.

The desired spacing, s_{des}, is the maximum among the following distance, s_{hw}, according to the time headway setting, the safe following distance, s_{safe}, considering the deceleration capabilities of the vehicles, and the minimum allowed distance, s_{min}, as described by:

$$\begin{cases} s_{des} = \max(s_{hw}, s_{safe}, s_{min}), \\ s_{hw} = v_f t_{hw}, \\ s_{safe} = \frac{v_f^2}{2}\left(\frac{1}{b_f^{max}} - \frac{1}{b_l^{max}}\right), \end{cases} \tag{3}$$

where s_{min} is the minimum clearance (2.0 m) in the standstill situation; t_{hw} is the system-specified time headway (s); and b_l^{max} and b_f^{max} are negative numbers indicating the maximum braking decelerations (m/s^2) of the leader and the follower, respectively.

The maximum safe speed v_f^{max} is an important constraint for avoiding rear-end collisions when the leading vehicle initiates emergency braking, which can be expressed as:

$$\begin{cases} v_f^{max} = \sqrt{-2b_f^{max} s_0}, \\ s_0 = (x_l - x_f - L) - v_f \tau - \frac{v_l^2}{2b_l^{max}}, \end{cases} \tag{4}$$

where x_l and L are the leading vehicle's position and exterior length, respectively.

C. Hybrid Powertrain Dynamics

Fig. 2 (left) shows the PHEV powertrain with a power-split configuration [27]. This system divides the engine power along two paths through a mechanical gear set; one path goes to the generator to produce electricity while the other one drives the wheels.

The planetary gear assembly consists of a planet carrier, a sun gear, and a ring gear, which are connected to the gasoline engine, the generator, and the reducer, respectively. Their torque balance is given by

$$\begin{cases} T_m = -(\frac{r_r}{r_s+r_r})T_e + \frac{1}{\kappa_c}T_d, \\ \omega_m = \kappa_c \omega_d, \\ T_g = -(\frac{r_r}{r_s+r_r})T_e, \\ \omega_e = (\frac{r_r}{r_s+r_r})\omega_m + (\frac{r_s}{r_s+r_r})\omega_g, \end{cases} \tag{5}$$

where T_e, T_m, and T_g indicate torques (N·m) that are respectively delivered from the engine, the motor and the generator; ω_e, ω_m, ω_g, and ω_d are respectively the angular velocities (rad/s) of the engine, the motor, the generator and the driveline; κ_c is the fixed gear ratio of the reducer; and r_s and r_r are respectively the radii of the sun gear and the ring gear.

The 1.5 L gasoline engine is modeled using its empirical performance map, as displayed in Fig. 2 (a). According to the data in the map, the instantaneous fuel consumption rate, $\dot{m}_f$ (g/s), is calculated by

$$\dot{m}_f = \frac{T_e \omega_e}{H_v \eta_e}, \tag{6}$$

where H_v is the lower heating value (J/g) of gasoline and η_e is the engine thermal efficiency.

The high voltage battery pack consists of lithium-ion 18650-type cells. The battery dynamics are governed by the following equations [35], [36]:

$$\begin{cases} P_b = V_{oc} I_b - I_b^2 R_{in}, \\ \dot{SoC} = -\frac{I_b}{Q_b} = -\frac{V_{oc} - \sqrt{V_{oc}^2 - 4R_{in}P_b}}{2R_{in}Q_b}, \end{cases} \tag{7}$$

where I_b and P_b are respectively the current (A) and the power (W) of the battery pack; R_{in} and V_{oc} respectively denote the internal resistance (Ω) and the open-circuit voltage (V), whose dynamic characteristics are displayed in Fig. 2 (b) (assuming batteries operate at a constant temperature of 35 °C); Q_b is the nominal capacity (A·s) of the battery pack. The battery SoC is subject to the constraints ($SoC \in [0.2, 0.8]$), to ensure safe

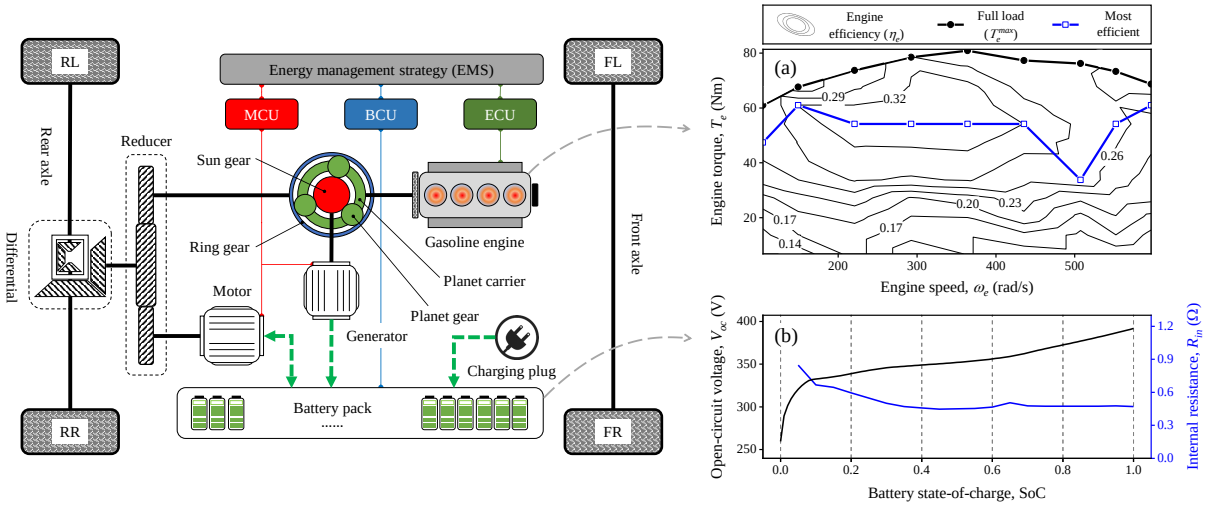

Fig. 2. The power-split PHEV powertrain (left) and the dynamics of the engine (a) and the battery pack (b).

battery operation and prolong its service life [37]. According to power balance, the battery power P_b is given by

$$P_b = \frac{\eta_m^{\kappa_m}}{r} T_d v_f - \eta_g T_e \omega_e - \frac{\kappa_c r_r (\eta_m^{\kappa_m} - \eta_g)}{r(r_r + r_s)} T_e v_f, \quad (8)$$

where η_m and η_g represent the efficiency factors of the motor and the generator, respectively. The motor can either drive the wheels ($\kappa_m = -1$) or charge the battery by performing regenerative braking ($\kappa_m = 1$).

TABLE I
MAIN SPECIFICATIONS OF THE POWER-SPLIT PHEV

Parameter	Value	Parameter	Value
m_0	1350 kg	r	0.28 m
A_f	2.2 m^2	ρ	1.225 kg/m^3
C_d	0.3	f	0.021
r_s	0.03 m	r_r	0.078 m
κ_c	3.9	Q_b	90000 A·s

D. Energy Management Strategy

Charge depleting - charge sustaining (CD-CS) is a well-proved EMS [38], taking advantage of the PHEV's extended all-electric (or zero-emissions) range and protecting battery cells from overcharge or overdischarge. Moreover, this strategy is favored by its simplicity and ease of implementation. According to the CD-CS model defined in our previously published study [39], the engine torque demand, T_e, is computed as a function of the engine speed, ω_e, and the battery SoC as follows:

$$T_e(SoC, \omega_e) = \begin{cases} 0, & SoC \in [\varepsilon_1, 1], \\ T_e^{max}(\omega_e) \cdot \exp\Big(- \frac{(SoC-\varepsilon_2)^2}{2\sigma^2} \Big), & SoC \in [\varepsilon_2, \varepsilon_1], \\ T_e^{max}(\omega_e), & SoC \in [0, \varepsilon_2], \end{cases} \quad (9)$$

where σ is a constant factor; ε_1 and ε_2 are two thresholds that are equal to 0.8 and 0.2, respectively; and T_e^{max} is the full-load torque of the engine, as shown in Fig. 2 (a). The PHEV main specifications mentioned in this section are summarized in Table I.

III. Problem Formulation and Optimization Methods

Fig. 3 gives an overview of the multi-objective CACC and EMS co-optimization problem. The decision vector (or solution), the objective vector (or outcome) and the state vector are exemplified in subplots. Different driving cycles of the leading vehicle are provided for optimization and validation purposes. The formulated optimization problem is solved by the Pareto method or the weighted-sum method (serving as a benchmark), by guiding a population of candidate solutions towards better solutions that simultaneously minimize multiple objectives.

A. Multi-objective Problem Formulation

Fig. 3 (c) indicates that the decision vector $K = [k_v, k_s, \sigma]$ consists of the principal control parameters in CACC and EMS systems. k_v and k_s are gain factors in equation (2), that determine the car-following behaviour; the variable, σ, in equation (9) governs the torque (or power) split. Previous studies [34], [39] have given the recommended value, K_{base} = [0.58, 0.10, 0.10], that is utilized as the baseline scheme in this work.

As an image of the decision vector K through the optimization algorithm, the objective vector $J = [J_1, J_2, J_3]$ is mainly concerned with tracking safety, ride comfort, and energy efficiency, as follows:

$$\begin{cases} \min\limits_K J_1 = \frac{1}{t_f} \int_0^{t_f} \|s(t) - s_{des}(t)\|_2 \, dt, \\ \min\limits_K J_2 = \frac{1}{t_f} \int_0^{t_f} \|a_f(t)\|_2 \, dt, \\ \min\limits_K J_3 = \frac{1}{1000\ t_f} \Big(\int_0^{t_f} \dot{m}_f(t) H_v \, dt \\ \qquad + \big(SoC(t_f) - SoC(0)\big) Q_b V_b \Big), \end{cases} \quad (10)$$

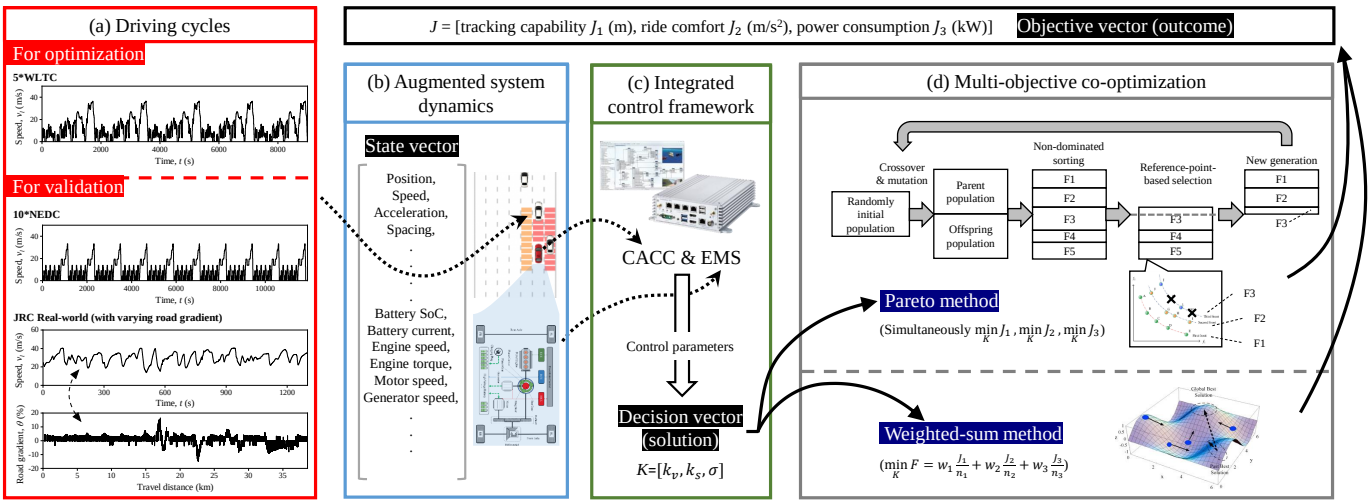

Fig. 3. Multi-objective co-optimization with the Pareto method and the weighted-sum method.

where t_f is the end time of the driving cycle adopted. Each element of the objective vector is defined as follows:

1) tracking capability, J_1, (m) is a 2-norm function of tracking error [40] and an important indicator for improving car-following safety and traffic throughput [41].
2) ride comfort, J_2, (m/s^2) is defined as a 2-norm function of the following vehicle's longitudinal acceleration. Although some studies utilize jerk as the indicator of ride comfort [24], acceleration is a more intuitive measure of the driver's sensation when driving on the road [32].
3) power consumption, J_3, (kW) is the average power demand to complete the driving cycle. The terms inside the parentheses represent the total energy consumption (J) including the consumed gasoline and the battery charge depletion [32].

Fig. 3 (a) shows the lead vehicle's driving cycles: 1) 5*WLTC indicates 5 consecutive repetitions of the worldwide harmonized light vehicle test cycle; 2) 10*NEDC means 10 consecutive repetitions of the new European driving cycle; 3) JRC Real-world, published by the European Commission - Joint Research Centre (JRC), is a highway driving trajectory with varying road gradient: this field test was conducted on a section of Autostrada A26 (Italy) between Ispra and Vicolungo, a 40-km trip, to collect driving data under actual traffic conditions. Among these driving cycles, the first one (5*WLTC) is applied in the multi-objective optimization process; the other two (10*NEDC and JRC Real-world) are utilized to validate the reliability and robustness of the resulting optimal solutions.

B. Multi-objective Optimization Methods

As demonstrated in Fig. 3 (d), the Pareto method and the weighted-sum method, for solving the above optimization problem, are two evolutionary algorithms (EAs) generating high-quality solutions by relying on bio-inspired operators such as mutation, crossover, and selection. However, the two methods have different selection schemes, i.e., different approaches to ordering the objective vectors in each generation.

1) Pareto method: For the formulated multi-objective CACC and EMS co-optimization problem, a single solution that simultaneously optimizes each objective is nonexistent. Instead, there exists a (possibly infinite) number of Pareto optimal solutions, in which one objective cannot be improved without degrading at least one of the other objectives. A solution K^1 is said to dominate (or Pareto) another solution K^2 (in notation, $K^1 \preceq K^2$) if the following conditions are met [31]:

$$\begin{cases} J_i(K^1) \leq J_i(K^2), \forall\ i \in [1,2,3], \\ J_j(K^1) < J_j(K^2), \exists\ j \in [1,2,3], \end{cases} \tag{11}$$

The solutions that are not dominated by others are called Pareto optimal K_{PF}. Their corresponding outcomes (or objective vectors J_{PF}) are represented by a Pareto frontier (PF). The high-level knowledge (e.g., trade-offs and scale differences between objectives) of the Pareto set (K_{PF}, J_{PF}) assists in finding a best-compromise solution. To find an approximation of the entire Pareto frontier, a non-dominated sorting genetic algorithm (NSGA-III) [42], [43] is employed in this work.

2) Weighted-sum method: Serving as a benchmark, the weighted-sum method integrates different objectives into a single cost function using configurable weights. After the scalarization, the objective vectors can be ordered as per the composite cost value. Mathematically, the weighted-sum method can be represented by

$$\min_K F = \sum_{i=1}^{3} w_i \frac{J_i(K)}{n_i} \text{ for } w_i \geq 0 \text{ and } \sum_{i=1}^{3} w_i = 1, \tag{12}$$

where w_i is the weight factor, and n_i is the normalization factor. Although this method is computationally efficient, the major limitation is that it cannot determine the factors w_i and n_i that can optimally balance and scale the objective functions for a problem with little or no information [31]. In this work,

a particle swarm optimization (PSO) algorithm [5] is applied to minimize the cost function, F, and find the corresponding optimal solution, K_{WS}.

IV. Results and Discussion

This section will be divided into four parts. Firstly, the Pareto frontier (K_{PF}, J_{PF}) reveals the high-level knowledge, e.g., trade-offs and scale differences between the objectives, for the CACC and EMS co-optimization problem. Secondly, the Pareto knowledge assists in finding a best-compromise solution K^*_{PF}, whose safety and energy benefits are validated by comparing with the baseline scheme (K_{base}) in various driving conditions. Thirdly, the weighted-sum optimal solutions with (K^P_{WS}) and without (K^B_{WS}) the Pareto knowledge, highlight that the weighted-sum method cannot optimally scale the objective functions if the Pareto information is unknown. Finally, we compare the sensitivities of the objective functions to variations in the reaction time, τ.

A. The Pareto Frontier

Fig. 4 shows the representative Pareto frontier (PF) approximated by NSGA-III. For visualization and analysis purposes, the three-dimensional (3D) objective vectors are projected onto the 2D scatter plots of Fig. 4 (a) - (c). The ideal (z^{ideal}) and the nadir (z^{nad}) vectors correspond to the lower and the upper boundaries, respectively. Fig. 4 (a) presents a trade-off between tracking capability, J_1, and ride comfort, J_2, since one of them will deteriorate when the other is improved on the PF. Fig. 4 (b) shows a similar relationship between tracking capability, J_1, and power consumption, J_3. However, Fig. 4 (c) demonstrates a harmonious relationship between ride comfort, J_2, and power consumption, J_3, because the reduction of any one is rewarded with a simultaneous decrease in the other. It also suggests that acceleration levels of the PHEV impact significantly on its energy consumption [41].

TABLE II
Marginal Distributions of Objectives on the Pareto Frontier

Objective	R_{PF}	Median
Tracking capability, J_1	0.094	0.194
Ride comfort, J_2	0.016	0.359
Power consumption, J_3	0.018	18.147

Marginal distributions of the objectives are illustrated by the box-whisker diagrams in Fig. 4 (d) - (f). The height of the box is the interquartile range (IQR) between the first quartile (Q_1, 25 %) and the third quartile (Q_3, 75 %). The median (the band inside the box) denotes the second quartile (Q_2, 50 %). The ends of the whisker represent the Pareto performance range ($R_{PF} = z^{nad} - z^{ideal}$). Table II summarizes the R_{PF} values and the medians of the PF, indicating that different objective functions are measured on different scales. For example, the median of power consumption, J_3, is two orders of magnitude larger than that of the tracking capability, J_1.

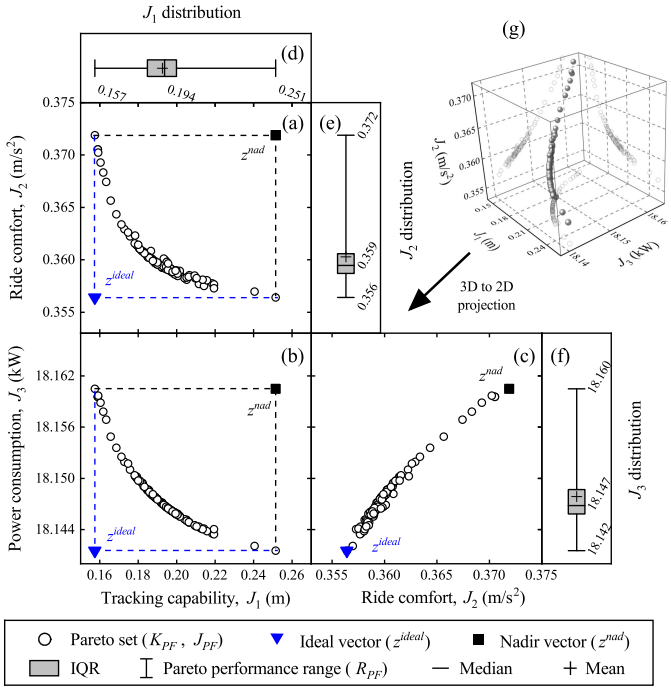

Fig. 4. The representative Pareto frontier (PF) approximated by NSGA-III.

B. Benefits of the Pareto Optimum

Usually, only one solution is required but all Pareto solutions (K_{PF}) are considered equally good because their objective vectors, J_{PF}, cannot be ordered directly. To find a best-compromise solution, a penalty function, u, utilizes the above high-level Pareto knowledge to rank the Pareto set [44]:

$$\min_{K\in PF} u\Big(J(K)\Big) = \min_{K\in PF} \sum_{i=1}^{3} w_i \frac{J_i(K) - z_i^{ideal}}{z_i^{nad} - z_i^{ideal}}, \qquad (13)$$

where z_i^{ideal} and z_i^{nad} adjust objectives measured on different scales to a notionally common scale; and the weight factor w_i represents the decision maker's preferences, whose value is assigned as $w = [0.5, 0.25, 0.25]$ to balance trade-offs between the objectives. Consequently, the Pareto solution with the minimum penalty, u, is the best-compromise one, K^*_{PF} = [1.22, 1.06, 0.05] in this study and defined as the Pareto optimum.

Fig. 5 draws a comparison between the Pareto optimum (K^*_{PF}) and the baseline scheme (K_{base}) in terms of their car-following and power-split performances in the 5*WLTC driving test. Fig. 5 (i) displays a zoomed portion of the inter-vehicle spacing, s, profiles of Fig. 5 (a). It can be seen from these two graphs that K^*_{PF} can always meet the minimum spacing requirement in equation (3), namely, $s \geq 2.0$ m; this constraint, however, is violated by the K_{base} control design. Moreover, Fig. 5 (b) shows that K^*_{PF} can significantly reduce tracking error, $s - s_{des}$, thus enhancing car-following safety. Fig. 5 (c) and (d) illustrate the following vehicle's speed and acceleration, respectively. Fig. 5 (e) - (h) compare the power-split dynamics of the two control schemes. For the K_{base} design, the engine and the

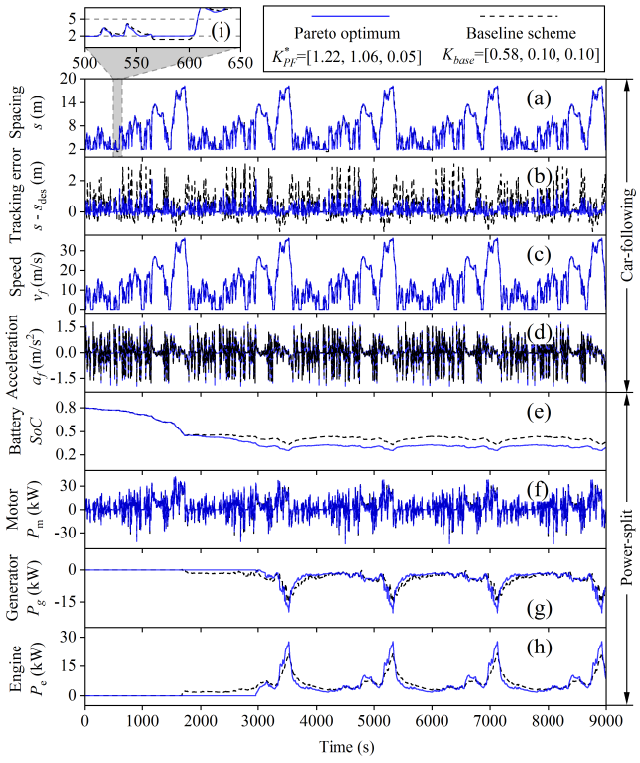

Fig. 5. The comparison of control performances between the Pareto optimum K^*_{PF} and the baseline scheme K_{base}.

generator started to work at $\sim$ 1700 s, i.e. switching to the CS mode; the battery SoC was then kept at $\sim$ 0.4. For the K^*_{PF} design, however, the CS mode was postponed until $\sim$ 3000 s and the battery SoC was controlled at the lower level of $\sim$ 0.3.

Table III compares the control performances, J_i between the Pareto optimum, K^*_{PF}, and the baseline scheme, K_{base}, in the optimization (5*WLTC) and validation (10*NEDC and JRC Real-world) driving cycles. The data highlight that the Pareto optimal solution for CACC and EMS design can provide considerable and consistent benefits in different driving conditions. For example, in the JRC Real-world driving cycle with varying road gradient, the Pareto optimum, K^*_{PF}, can reduce energy consumption (by 7.57 %) and tracking error (by 68.94 %), while at the same time satisfying ride comfort needs.

C. Weighted-sum Optimums

Serving as a benchmark, the weighted-sum method uses the same weight vector, $w = [0.5, 0.25, 0.25]$, as the Pareto method to balance the trade-offs between the objectives. For comparison purposes, the weighted-sum method in this work utilizes two different normalization techniques [45]:

1) Normalization (without the Pareto knowledge) by objective values at the baseline point, $n = J(K_{base})$. The corresponding weighted-sum optimum is (K^B_{WS}, J^B_{WS}).
2) Normalization (with the Pareto knowledge) by the Pareto performance range, $n = R_{PF} = z^{nad} - z^{ideal}$. The corresponding weighted-sum optimum is (K^P_{WS}, J^P_{WS}).

Fig. 6 (a) - (c) illustrate the evolutions of J^P_{WS} and J^B_{WS} during 30 PSO iterations. It is obvious that the weighted-sum method is computationally efficient because the objectives converged rapidly (within 20 generations). However, different normalization techniques lead to different final optimums. In Fig. 6 (d) - (f), the weighted-sum optimums are projected onto 2D planes and compared with the Pareto frontier (PF). It is worth noting that J^P_{WS} is located on the PF and very close to the Pareto optimum, J^*_{PF}. In contrast, J^B_{WS} presents an over-optimized tracking capability, J_1, which can, in turn, compromise the other performance measures, i.e. the ride comfort, J_2, and the power consumption, J_3. Table IV summarizes the final optima through the Pareto method as well as the weighted-sum methods with differing normalization.

These comparisons reveal that the weighted-sum method cannot determine the normalization factors that can optimally scale the objective functions if the high-level Pareto knowledge is unknown before the optimization begins. The Pareto method can overcome this limitation by producing a set of Pareto optimal solutions. These solutions indicate trade-offs and scale differences between objectives and assist in finding a best-compromise solution that can accurately capture the decision maker's preferences.

D. Sensitivities to the Reaction Time

Encompassing communication, sensing and actuation delays, the reaction time, τ, in (2) and (4) is a major factor that impacts tracking safety, ride comfort, and fuel economy. This section demonstrates the sensitivities of the objectives to τ variations and compares the performance robustness of the Pareto and the weighted-sum optima.

The sensitivity of each objective to the reaction time variation can be calculated by [5]

$$S_{i,j} = \left| \frac{\big(J_i(\tau_j) - J_i(\tau_0)\big)/J_i(\tau_0)}{(\tau_j - \tau_0)/\tau_0} \right|, \tag{14}$$

where $S_{i,j}$ is the sensitivity of the objective J_i (i = 1, 2, 3) to the variation of the reaction time, $\tau_j \in [0.3, 0.4, 0.5, 0.6]$ s. $J_i(\tau_0)$ is chosen as the reference corresponding to the situation when $\tau_j = \tau_0 = 0.3$ s. The larger the sensitivity value, the more significant the influence of reaction time on the outcome.

In Fig. 7, the tracking capability (J_1) shows the highest sensitivity to variation in τ. Its sensitivity, $S_{1,j}$, increases with increasing reaction time. The power consumption, J_3, is the least sensitive criterion, whose sensitivity is two orders of magnitude smaller than that of J_1. Therefore, the reaction time impacts significantly on tracking safety, but its effect on energy saving is trivial. In addition, compared with the weighted-sum counterpart, K^B_{WS}, the Pareto optimum, K^*_{PF}, always exhibits less sensitivity to τ variation for every objective, indicating a higher level of performance robustness against a range of operational delays in various driving scenarios.

TABLE III
THE BENEFITS OF THE PARETO OPTIMUM K^*_{PF}

	5*WLTC			10*NEDC			JRC Real-world		
	J_1 (m)	J_2 (m/s^2)	J_3 (kW)	J_1 (m)	J_2 (m/s^2)	J_3 (kW)	J_1 (m)	J_2 (m/s^2)	J_3 (kW)
K_{base}	0.5640	0.3638	19.2638	0.3710	0.2588	12.9026	0.9462	0.4831	47.5019
K^*_{PF}	0.1858	0.3602	18.1484	0.0936	0.2634	11.7137	0.2939	0.4915	43.9082
Reduction (%)	67.06	0.99	5.79	74.77	-1.78	9.21	68.94	-1.74	7.57

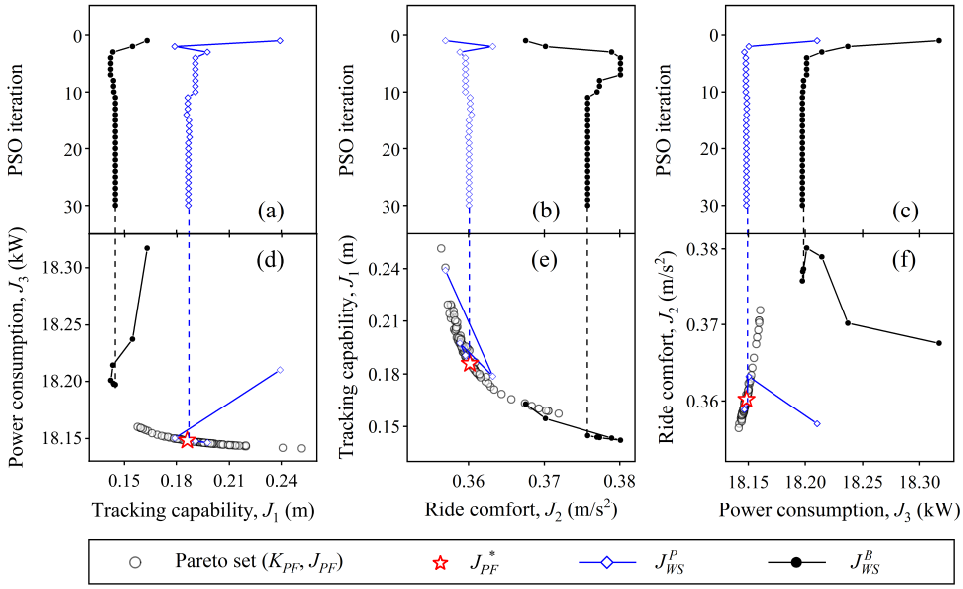

Fig. 6. Multi-objective optimization using weighted-sum methods.

TABLE IV
THE COMPARISON OF THE PARETO AND THE WEIGHTED-SUM OPTIMUMS IN THE 5*WLTC DRIVING TEST

	K^*_{PF} [1.22, 1.06, 0.05]	K^P_{WS} [1.23, 1.06, 0.05]	K^B_{WS} [1.89, 2.49, 0.05]
J_1 (m)	0.1858	0.1864	0.1447
J_2 (m/s^2)	0.3602	0.3601	0.3758
J_3 (kW)	18.1484	18.1483	18.1976
Penalty u	30.2384	30.2640	50.0000

V. CONCLUSIONS

In vehicle control design, the co-optimization of electrification, automation, and connectivity is gaining traction among automakers and policymakers. Previous approaches such as weighted-sum methods overlook trade-offs and scale differences inherent in these multi-objective problems, resulting in misleading optimizations. To overcome these limitations, this study proposes a Pareto-based framework demonstrated to optimize system parameters of cooperative adaptive cruise control (CACC) and energy management strategy (EMS) for PHEVs. The high-level knowledge of the Pareto frontier (PF) assists in finding a best-compromise solution. The optimized systems can be directly applied in real applications. The results of this study are as follows:

1) The Pareto frontier suggests that the comfort and the energy targets are harmonious, but they both conflict with the safety target. Their objective values are measured on different scales.
2) In the validation using real-world driving data, the Pareto optimum, K^*_{PF}, for CACC and EMS systems,

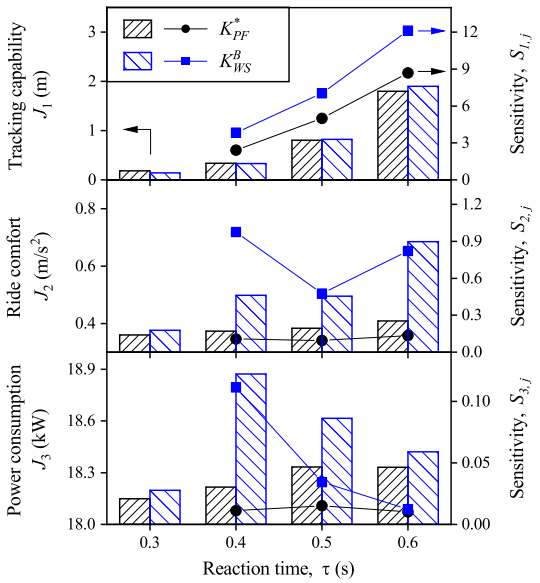

Fig. 7. Sensitivities of the objectives to reaction time τ variations.

compared with the baseline scheme, K_{base}, can reduce energy consumption (by 7.57 %) and tracking error (by 68.94 %), while at the same time satisfying ride comfort needs.

3) In contrast to the weighted-sum method, the proposed Pareto method can optimally balance and scale the multiple objective functions and thus accurately capture the decision maker's preferences.
4) Sensitivity analysis proves that the vehicle reaction time impacts significantly on tracking safety, but its effect on energy saving is trivial.

ACKNOWLEDGMENT

This work was based on a collaboration agreement between the University of Birmingham and the Joint Research Centre of the European Commission. The authors are grateful to Biagio Ciuffo for his support during this project.

REFERENCES

[1] M. Alonso Raposo, B. Ciuffo, F. Ardente, J. Aurambout, G. Baldini, R. Braun, and I. Vandecasteele, "The future of road transport: Implications of automated, connected, low-carbon and shared mobility," *European Commission - Joint Research Centre (JRC)*, 2019.

[2] G. J. Offer, "Automated vehicles and electrification of transport," *Energy & Environmental Science*, vol. 8, no. 1, pp. 26–30, 2015.

[3] L. Zhang, Y. Wang, and Z. Wang, "Robust lateral motion control for in-wheel-motor-drive electric vehicles with network induced delays," *IEEE Transactions on Vehicular Technology*, 2019.

[4] Y. Wang, Z. Wang, L. Zhang, M. Liu, and J. Zhu, "Lateral stability enhancement based on a novel sliding mode prediction control for a four-wheel-independently actuated electric vehicle," *IET Intelligent Transport Systems*, vol. 13, no. 1, pp. 124–133, 2018.

[5] Q. Zhou, W. Zhang, S. Cash, O. Olatunbosun, H. Xu, and G. Lu, "Intelligent sizing of a series hybrid electric power-train system based on chaos-enhanced accelerated particle swarm optimization," *Applied Energy*, vol. 189, pp. 588–601, 2017.

[6] Q. Zhou, J. Li, B. Shuai, H. Williams, Y. He, Z. Li, H. Xu, and F. Yan, "Multi-step reinforcement learning for model-free predictive energy management of an electrified off-highway vehicle," *Applied Energy*, vol. 255, p. 113755, 2019.

[7] J. Li, Q. Zhou, H. Williams, and H. Xu, "Back-to-back competitive learning mechanism for fuzzy logic based supervisory control system of hybrid electric vehicles," *IEEE Transactions on Industrial Electronics*, 2019.

[8] J. Li, Q. Zhou, Y. He, B. Shuai, Z. Li, H. Williams, and H. Xu, "Dual-loop online intelligent programming for driver-oriented predict energy management of plug-in hybrid electric vehicles," *Applied Energy*, vol. 253, p. 113617, 2019.

[9] M. Makridis, K. Mattas, and B. Ciuffo, "Response time and time headway of an adaptive cruise control. an empirical characterization and potential impacts on road capacity," *IEEE Transactions on Intelligent Transportation Systems*, 2019.

[10] B. Ciuffo, M. Makridis, T. Toledo, and G. Fontaras, "Capability of current car-following models to reproduce vehicle free-flow acceleration dynamics," *IEEE Transactions on Intelligent Transportation Systems*, vol. 19, no. 11, pp. 3594–3603, 2018.

[11] V. Milanés and S. E. Shladover, "Modeling cooperative and autonomous adaptive cruise control dynamic responses using experimental data," *Transportation Research Part C: Emerging Technologies*, vol. 48, pp. 285–300, 2014.

[12] L. Guo, H. Chen, Q. Liu, and B. Gao, "A computationally efficient and hierarchical control strategy for velocity optimization of on-road vehicles," *IEEE Transactions on Systems, Man, and Cybernetics: Systems*, vol. 49, no. 1, pp. 31–41, 2018.

[13] C. M. Martinez, X. Hu, D. Cao, E. Velenis, B. Gao, and M. Wellers, "Energy management in plug-in hybrid electric vehicles: Recent progress and a connected vehicles perspective," *IEEE Transactions on Vehicular Technology*, vol. 66, no. 6, pp. 4534–4549, 2016.

[14] F. Zhang, X. Hu, R. Langari, and D. Cao, "Energy management strategies of connected HEVs and PHEVs: Recent progress and outlook," *Progress in Energy and Combustion Science*, vol. 73, pp. 235–256, 2019.

[15] D. Maamria, K. Gillet, G. Colin, Y. Chamaillard, and C. Nouillant, "Computation of eco-driving cycles for hybrid electric vehicles: Comparative analysis," *Control Engineering Practice*, vol. 71, pp. 44–52, 2018.

[16] G. Heppeler, M. Sonntag, U. Wohlhaupter, and O. Sawodny, "Predictive planning of optimal velocity and state of charge trajectories for hybrid electric vehicles," *Control Engineering Practice*, vol. 61, pp. 229–243, 2017.

[17] L. Guo, B. Gao, Y. Gao, and H. Chen, "Optimal energy management for HEVs in eco-driving applications using bi-level MPC," *IEEE Transactions on Intelligent Transportation Systems*, vol. 18, no. 8, pp. 2153–2162, 2016.

[18] J. Hu, Y. Shao, Z. Sun, M. Wang, J. Bared, and P. Huang, "Integrated optimal eco-driving on rolling terrain for hybrid electric vehicle with vehicle-infrastructure communication," *Transportation Research Part C: Emerging Technologies*, vol. 68, pp. 228–244, 2016.

[19] A. Plianos, T. Jokela, and M. Hancock, "Predictive energy optimization for connected and automated HEVs," SAE Technical Paper, Tech. Rep., 2018.

[20] G. Li and D. Görges, "Ecological adaptive cruise control and energy management strategy for hybrid electric vehicles based on heuristic dynamic programming," *IEEE Transactions on Intelligent Transportation Systems*, 2018.

[21] M. Vajedi and N. L. Azad, "Ecological adaptive cruise controller for plug-in hybrid electric vehicles using nonlinear model predictive control," *IEEE Transactions on Intelligent Transportation Systems*, vol. 17, no. 1, pp. 113–122, 2015.

[22] B. Sakhdari, M. Vajedi, and N. L. Azad, "Ecological adaptive cruise control of a plug-in hybrid electric vehicle for urban driving," in *2016 IEEE 19th International Conference on Intelligent Transportation Systems (ITSC)*. IEEE, 2016, pp. 1739–1744.

[23] S. Xie, X. Hu, T. Liu, S. Qi, K. Lang, and H. Li, "Predictive vehicle-following power management for plug-in hybrid electric vehicles," *Energy*, vol. 166, pp. 701–714, 2019.

[24] L. Li, X. Wang, and J. Song, "Fuel consumption optimization for smart hybrid electric vehicle during a car-following process," *Mechanical Systems and Signal Processing*, vol. 87, pp. 17–29, 2017.

[25] S. Qiu, L. Qiu, L. Qian, and P. Pisu, "Hierarchical energy management control strategies for connected hybrid electric vehicles considering efficiencies feedback," *Simulation Modelling Practice and Theory*, vol. 90, pp. 1–15, 2019.

[26] M. Ghasemi and X. Song, "Powertrain energy management for autonomous hybrid electric vehicles with flexible driveline power demand," *IEEE Transactions on Control Systems Technology*, 2018.

[27] G. Ma, M. Ghasemi, and X. Song, "Integrated powertrain energy management and vehicle coordination for multiple connected hybrid electric vehicles," *IEEE Transactions on Vehicular Technology*, vol. 67, no. 4, pp. 2893–2899, 2017.

[28] M. Hovgard, O. Jonsson, N. Murgovski, M. Sanfridson, and J. Fredriksson, "Cooperative energy management of electrified vehicles on hilly roads," *Control Engineering Practice*, vol. 73, pp. 66–78, 2018.

[29] B. Chen, S. A. Evangelou, and R. Lot, "Series hybrid electric vehicle simultaneous energy management and driving speed optimization," *IEEE/ASME Transactions on Mechatronics*, 2019.

[30] J. Borek, B. Groelke, C. Earnhardt, and C. Vermillion, "Economic optimal control for minimizing fuel consumption of heavy-duty trucks in a highway environment," *IEEE Transactions on Control Systems Technology*, 2019.

[31] M. Awad and R. Khanna, "Multiobjective optimization," in *Efficient Learning Machines*. Springer, 2015, pp. 185–208.

[32] Y. Luo, T. Chen, S. Zhang, and K. Li, "Intelligent hybrid electric vehicle ACC with coordinated control of tracking ability, fuel economy, and ride comfort," *IEEE Transactions on Intelligent Transportation Systems*, vol. 16, no. 4, pp. 2303–2308, 2015.

[33] B. Van Arem, C. J. Van Driel, and R. Visser, "The impact of cooperative adaptive cruise control on traffic-flow characteristics," *IEEE Transactions on intelligent transportation systems*, vol. 7, no. 4, pp. 429–436, 2006.

[34] H. S. Mahmassani, "50th anniversary invited article - autonomous vehicles and connected vehicle systems: Flow and operations considerations," *Transportation Science*, vol. 50, no. 4, pp. 1140–1162, 2016.

[35] T. Liu, X. Hu, S. E. Li, and D. Cao, "Reinforcement learning optimized look-ahead energy management of a parallel hybrid electric vehicle,"

IEEE/ASME Transactions on Mechatronics, vol. 22, no. 4, pp. 1497–1507, 2017.

[36] K. Wu, M. Kuang, M. Milacic, X. Zhang, and J. Sun, "Analysis of effects of fuel cell system dynamics on optimal energy management," in *ASME 2017 Dynamic Systems and Control Conference*. American Society of Mechanical Engineers, 2017.

[37] X. Hu, C. M. Martinez, and Y. Yang, "Charging, power management, and battery degradation mitigation in plug-in hybrid electric vehicles: A unified cost-optimal approach," *Mechanical Systems and Signal Processing*, vol. 87, pp. 4–16, 2017.

[38] Z. Chen, R. Xiong, C. Wang, and J. Cao, "An on-line predictive energy management strategy for plug-in hybrid electric vehicles to counter the uncertain prediction of the driving cycle," *Applied Energy*, vol. 185, pp. 1663–1672, 2017.

[39] Q. Zhou, Y. Zhang, Z. Li, J. Li, H. Xu, and O. Olatunbosun, "Cyber-physical energy-saving control for hybrid aircraft-towing tractor based on online swarm intelligent programming," *IEEE Transactions on Industrial Informatics*, vol. 14, no. 9, pp. 4149–4158, 2017.

[40] D. Corona, M. Lazar, B. De Schutter, and M. Heemels, "A hybrid MPC approach to the design of a smart adaptive cruise controller," in *IEEE International Conference on Control Applications*. IEEE, 2006, pp. 231–236.

[41] S. Li, K. Li, R. Rajamani, and J. Wang, "Model predictive multi-objective vehicular adaptive cruise control," *IEEE Transactions on Control Systems Technology*, vol. 19, no. 3, pp. 556–566, 2010.

[42] K. Deb and H. Jain, "An evolutionary many-objective optimization algorithm using reference-point-based nondominated sorting approach, part I: Solving problems with box constraints," *IEEE Transactions on Evolutionary Computation*, vol. 18, no. 4, pp. 577–601, 2013.

[43] H. Jain and K. Deb, "An evolutionary many-objective optimization algorithm using reference-point based nondominated sorting approach, part II: Handling constraints and extending to an adaptive approach," *IEEE Transactions on Evolutionary Computation*, vol. 18, no. 4, pp. 602–622, 2013.

[44] S. H. R. Pasandideh and S. T. A. Niaki, "Multi-response simulation optimization using genetic algorithm within desirability function framework," *Applied Mathematics and Computation*, vol. 175, no. 1, pp. 366–382, 2006.

[45] Z. Chen and S. Andresen, "A multiobjective optimization model of production-sourcing for sustainable supply chain with consideration of social, environmental, and economic factors," *Mathematical Problems in Engineering*, vol. 2014, 2014.

Yinglong He received the B.Eng. and M.Res. degrees in energy and power engineering from Huazhong University of Science and Technology, Wuhan, China, in 2014 and 2017, respectively. He is currently a scholarship-funded Ph.D. candidate with the Intelligent Vehicle Control Team in the University of Birmingham, Birmingham, UK. His current research interests include intelligent transportation, vehicle dynamics, driver behavior, multi-objective optimization and machine learning.

Quan Zhou received the B.Eng. and M.Res. degrees (Hons) in vehicle engineering from Wuhan University of Technology, Wuhan, China, in 2012 and 2015, respectively. He is currently a Research Fellow at the Intelligent Vehicle Control Team, Vehicle and Engine Technology Research Centre, University of Birmingham, Birmingham, U.K. His research interests include vehicle system modeling, HEV/EV design optimization, optimal control, and artificial intelligence for future HEVs and CAVs.

Michail Makridis received the Ph.D. degree in image processing and machine intelligence from the Democritus University of Thrace, Greece. Since 2012, he has been with the European Commission Joint Research Centre as a Researcher and a Science and Policy Officer. His interests are in intelligent transportation systems, simulation of vehicle dynamics and driver behavior, energy demand and emissions, image segmentation and classification, natural language processing, and sequential pattern mining. He is a Reviewer in international journals and author of various publications in the fields of traffic modeling and simulation, image processing, and machine learning.

Konstantinos Mattas is a Ph.D. candidate of the Democritus University of Thrace in Xanthi, Greece, working on fuzzy logic applications in transportation engineering. He holds a M.Sc. in applied mathematics from the same university and a civil engineering degree, specialized in transportation. Since 2017 he is working with the European Commission Joint Research Centre. His interests are in intelligent transportation systems, simulation of vehicle dynamics and driver behavior, microscopic simulation of traffic networks and network control, optimization and traffic safety.

Ji Li received the B.Eng. degree in engineering from the Chongqing University of Technology, Chongqing, China, in 2015. He is currently a Ph.D. candidate in the Intelligent Vehicle System and Control Team, University of Birmingham, Birmingham, U.K. His current research interests include fuzzy mathematics, deep reinforcement learning, transfer learning, and development of driving behavior recognition, human machine interaction and vehicle systems optimization.

Huw Williams received a bachelor's degree in mathematics from the University of Oxford, and a Ph.D. in theoretical mechanics from the University of East Anglia. He has over 20 years' experience in the automotive industry. Huw joined Jaguar Land Rover in 1986 where he worked in research and development applying mathematical modeling techniques to all aspects of vehicle technology. He is both a chartered fellow of the Institute of Mathematics and its Applications and a fellow of the Royal Statistical Society.

Hongming Xu received the Ph.D. degree in mechanical engineering from Imperial College London, London, U.K. He is a Professor of Energy and Automotive Engineering at the University of Birmingham, Birmingham, U.K., and the Head of Vehicle and Engine Technology Research Centre. He has six years of industrial experience with Jaguar Land Rover and Premier Automotive Group of Ford. He has authored and co-authored more than 300 journal and SAE technical publications on advanced vehicle powertrain systems involving both experimental and modeling studies. He is a Fellow of SAE International and IMechE.